Association of aerobic glycolysis with the structural connectome reveals a benefit–risk balancing mechanism in the human brain

Yuhan Chen[a,b,c], Qixiang Lin[a,b,c], Xuhong Liao[a,b,c,d], Changsong Zhou[e,f,g,h,i,j,1], and Yong He[a,b,c,k,1]

[a]State Key Laboratory of Cognitive Neuroscience and Learning, Beijing Normal University, Beijing 100875, China; [b]Beijing Key Laboratory of Brain Imaging and Connectomics, Beijing Normal University, Beijing 100875, China; [c]International Data Group (IDG)/McGovern Institute for Brain Research, Beijing Normal University, Beijing 100875, China; [d]School of Systems Science, Beijing Normal University, Beijing 100875, China; [e]Department of Physics, Hong Kong Baptist University, Kowloon Tong, Hong Kong, China; [f]Centre for Nonlinear Studies, Institute of Computational and Theoretical Studies, Hong Kong Baptist University, Kowloon Tong, Hong Kong, China; [g]Beijing–Hong Kong–Singapore Joint Centre for Nonlinear and Complex Systems (Hong Kong), Institute of Computational and Theoretical Studies, Hong Kong Baptist University, Kowloon Tong, Hong Kong, China; [h]Research Centre, Institute of Research and Continuing Education, Hong Kong Baptist University, Shenzhen 518000, China; [i]Beijing Computational Science Research Center, Beijing 100084, China; [j]Department of Physics, Zhejiang University, Hangzhou 310027, China; and [k]Chinese Institute for Brain Research, Beijing 102206, China

Edited by Marcus E. Raichle, Washington University in St. Louis, St. Louis, MO, and approved November 16, 2020 (received for review June 26, 2020)

Aerobic glycolysis (AG), that is, the nonoxidative metabolism of glucose, contributes significantly to anabolic pathways, rapid energy generation, task-induced activity, and neuroprotection; yet high AG is also associated with pathological hallmarks such as amyloid-β deposition. An important yet unresolved question is whether and how the metabolic benefits and risks of brain AG is structurally shaped by connectome wiring. Using positron emission tomography and magnetic resonance imaging techniques as well as computational models, we investigate the relationship between brain AG and the macroscopic connectome. Specifically, we propose a weighted regional distance-dependent model to estimate the total axonal projection length of a brain node. This model has been validated in a macaque connectome derived from tract-tracing data and shows a high correspondence between experimental and estimated axonal lengths. When applying this model to the human connectome, we find significant associations between the estimated total axonal projection length and AG across brain nodes, with higher levels primarily located in the default-mode and prefrontal regions. Moreover, brain AG significantly mediates the relationship between the structural and functional connectomes. Using a wiring optimization model, we find that the estimated total axonal projection length in these high-AG regions exhibits a high extent of wiring optimization. If these high-AG regions are randomly rewired, their total axonal length and vulnerability risk would substantially increase. Together, our results suggest that high-AG regions have expensive but still optimized wiring cost to fulfill metabolic requirements and simultaneously reduce vulnerability risk, thus revealing a benefit–risk balancing mechanism in the human brain.

default mode | connectomics | metabolism | neuroimaging | computational models

The human brain is a highly complex system that requires energy metabolism as well as structural and functional connectivity to maintain normal function (1–5). Aerobic glycolysis (AG) refers to the nonoxidative metabolism of glucose despite the presence of adequate oxygen. In the resting adult human brain, the topography of AG exhibits a large regional variation, with significantly elevated levels in the medial and lateral parietal as well as the prefrontal cortices (6). Brain AG is particularly crucial for biosynthesis (7, 8), rapid production of ATP (9), task-induced activity (10), synaptic plasticity (e.g., synapse formation and growth) (11), and neuroprotection against oxidative stress (12). However, research suggests that higher levels of brain AG could be associated with higher risk of pathological hallmarks such as amyloid-β deposition (10, 13). Specifically, high-AG regions in young adults correspond to those regions that are later most vulnerable to amyloid-β deposition (14) and even subthreshold amyloid-β deposition (13). Thus, brain AG appears to have a dual role, playing both a positive role in maintaining the metabolic requirements of normal function, while also at the same time presenting a risk of vulnerability. In the present study, we approach brain AG from a mechanistic perspective, and investigate whether there is a basis in the underlying structural connectome that can account for the dual effects generated by AG in the brain.

At the microscopic level, AG plays a vital role in the anabolic process (8). Specifically, AG produces acetyl CoA, a precursor for both fatty acid synthesis in myelination (15, 16) and amino acid synthesis in axonal elongation (17, 18). A metabolic transfer from the glycolytic oligodendroglia to the axons is necessary for long-term axonal integrity (9, 19–21). Moreover, AG alone is sufficient to support the maintenance of myelin in adulthood (9, 22, 23). Based on experimental observations of neuropathy (24) and animal models (25), researchers suggest that trophic support through glycolysis is wiring distance dependent, with longer axons associated with higher AG (26). These factors imply a tight association between AG and microscopic axonal structure. At

Significance

Aerobic glycolysis (AG) is the nonoxidative metabolism of glucose despite abundant oxygen. High AG is critical for various biological processes in the brain, such as biosynthesis and rapid ATP production, but also identifies regions most vulnerable to amyloid-β deposition. Currently, the wiring mechanisms underlying the metabolic benefits and risks of AG are largely unknown. Using advanced neuroimaging techniques and computational modelling, we systematically examined the relationship between AG and the connectome. Our results delineate large yet optimized wiring costs in high-AG regions (e.g., default-mode and prefrontal cortices), revealing a balancing mechanism that satisfies metabolic demand while reducing vulnerability risk. This research highlights wiring rules in high-AG regions and deepens our understanding of the relationship between brain metabolism and the connectome.

Author contributions: Y.C., C.Z., and Y.H. designed research; Y.C., Q.L., and X.L. performed research; Y.C. and Y.H. contributed new reagents/analytic tools; Y.C., Q.L., and X.L. analyzed data; and Y.C., C.Z., and Y.H. wrote the paper.

The authors declare no competing interest.

This article is a PNAS Direct Submission.

[1]To whom correspondence may be addressed. Email: cszhou@hkbu.edu.hk or yong.he@bnu.edu.cn.

This article contains supporting information online at https://www.pnas.org/lookup/suppl/doi:10.1073/pnas.2013232118/-/DCSupplemental.

Published December 21, 2020.

the macroscopic level, high-AG regions tend to be highly centralized or part of the rich club in the structural network of the human brain (1, 27). This provides initial evidence for establishing a connection between regional AG levels and network topology. However, whether and how brain AG is structurally shaped by connectome wiring remains largely unknown.

High-AG regions, which are primarily located in the default-mode and prefrontal cortices, largely overlap with brain hubs that are responsible for global communication (28–30). These regions also contain rich structural connections with other brain regions through axonal projections (31). From a supply–demand perspective, such regions require high glycolysis metabolism to support the large number of interregional axonal projections that are important for functional integration. However, high AG in the brain may carry a high risk of vulnerability. Specifically, studies of animal models in Alzheimer's disease (AD) suggest an association between neuronal activity, lactate levels, and amyloid-β concentration in the brain (32, 33). During normal aging, the human brain undergoes topographic changes and a global loss of AG, with the greatest decline observed in areas corresponding to high-AG regions in young adult brains (34). As AG protects the brain from reactive oxygen species to prevent oxidative stress (12, 35, 36), the reduced levels of AG in the aging brain means a loss of neuroprotection, which may be one of factors that consequently leads to a higher risk of amyloid-β accumulation (37, 38). Meanwhile, as misfolded proteins are toxic to neurons, this may lead to a further loss of AG. Increasing evidence suggests that high-AG regions in healthy brains correspond to those regions that are highly vulnerable to amyloid-β deposition (14) and that may even constitute the main sites for early on-target subthreshold amyloid deposition (13). Therefore, from a risk control perspective, AG levels in these high-AG regions should not be further increased. This poses an interesting question in relation to the wiring mechanism in high-AG regions, specifically, whether these regions have a wiring-optimized design that avoids the need for even higher AG (i.e., which would otherwise be needed to support the longer axonal projections) and creating the potential for higher vulnerability risk.

Based on these considerations, we hypothesized that high-AG regions in the human brain have large total axonal projection lengths to support functional integration between regions but that their wiring costs are optimized to avoid potentially high-risk situations created by excessive levels of AG. To address this hypothesis, we gathered two principal brain imaging datasets, the first set being positron emission tomography (PET) data (6), and the second set being high angular-resolution diffusion imaging (HARDI) and resting-state functional MRI (rsfMRI) data from the Human Connectome Project (HCP) (39). Here, PET data were applied to measure regional AG variations in the resting human brain, while HARDI and rsfMRI data were used respectively to acquire the brain's structural and functional connectomes. Specifically, we proposed a computational model based on regional distance-dependent weights to estimate the structural wiring cost of a brain node by approximately capturing the total length of its axonal projections in the connectome. Such an approach was validated in a macaque structural connectome derived from tract-tracing data. Furthermore, we performed a mediation analysis to explore whether brain AG significantly mediates the relationship between the estimated regional total projection length and functional integration. To determine whether structural wiring costs in high-AG regions are optimized to reduce the risk of vulnerability, we compared the estimated regional total projection lengths in the structural connectome with those derived from either wiring-optimized or randomized network models. Studying the structural wiring rules underlying brain AG topography has important implications for understanding how the human brain allocates metabolic resources to achieve a benefit–risk balance.

Results

Brain AG Is Significantly Correlated with Estimated Regional Axonal Projection Lengths in the Connectome. To study the relationship between brain AG and connectome wiring, we first divided the human cerebral cortex into 1,024 nodes (512 for each hemisphere) based on a randomized parcellation procedure (40). Using PET data from normal young adults (n = 33) (6), we measured brain AG levels in each of the 1,024 network nodes (for details, see *SI Appendix*, section 1.1). As reported previously (6), brain AG varies regionally in the resting state, with elevated levels primarily distributed bilaterally in the dorsolateral prefrontal cortex, superior and medial frontal gyrus, precuneus and posterior cingulate cortex, and inferior parietal lobes (Fig. 1*A*). According to Yeo's functional parcellation atlases (41), these high-AG regions mostly reside in the default-mode and cognitive control systems (Fig. 1*B*).

Furthermore, we proposed a computational model to estimate the regional total axonal projection length (rTAPL) of each brain node. In previous macroscopic human connectome studies, the wiring cost of a given brain region is usually defined by measuring the streamline number (42), streamline length (43), Euclidean distance (44), and combinations thereof (45) based on in vivo diffusion MRI tractography methods (*SI Appendix*, section 2). These measures, however, are inappropriate for capturing the total length of the axonal projections within a brain region (46, 47). To overcome this limitation, in the current study, we proposed a weighted regional distance-dependent model to estimate the total axonal projection length of each brain node within the structural connectome at a macroscale. This model was inspired by previous studies revealing that the interareal connection weights within a single hemisphere follow an exponential decay rule with Euclidean distance in primate species (48, 49). Briefly, in the present study, for each hemisphere, we used high-quality HCP HARDI data (39) and deterministic tractography approaches to reconstruct a population-based, binarized structural connectome "backbone" of the human brain with 512 nodes and 3.5% connectivity density (*SI Appendix*, section 1.2). For a given brain node i, we estimated total length of its axonal projections using the computational model $\mathrm{rTAPL}_i = \exp(-\alpha\langle d\rangle_i) \times D_i$. In this model, D_i denotes the total Euclidean distance of the connections linking node i to the rest of the network, $\exp(-\alpha\langle d\rangle_i)$ denotes the regional (nodal) effective weight that characterizes the normalized number of axonal projections associated with node i, $\langle d\rangle_i$ denotes the average Euclidean distance ($\langle d\rangle_i = D_i/K_i$, where K_i is the nodal degree) of the connections linking node i, and α is a tunable exponent parameter that represents the rate of decay of the regional effective weight with respect to distance. Before applying this model to the human connectome, we first performed a validation using the macroscopic macaque connectome derived from

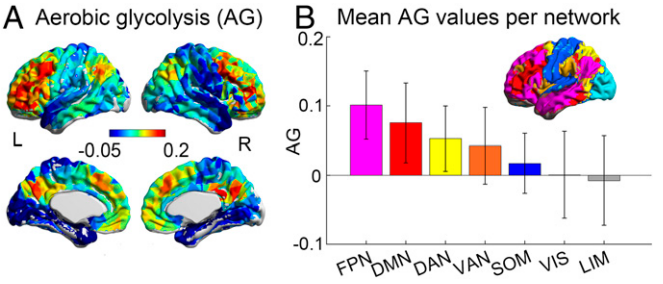

Fig. 1. Aerobic glycolysis in the human brain. (*A*) Map of aerobic glycolysis (AG) in the human brain. (*B*) Mean AG values within each functional brain network. The network subdivisions (inner panel) were obtained based on Yeo's parcellations (41). Error bars indicate the SD within each network. DAN, dorsal attention; DMN, default mode; FPN, frontoparietal; L, left hemisphere; LIM, limbic; R, right hemisphere; SOM, somatomotor; VAN, ventral attention; VIS, visual.

tract-tracing data (Fig. 2 *A* and *B*) (50) (for details, see *SI Appendix*, section 3.1–3.3). We observed significant correlations ($r = 0.80$, $P < 1.0 \times 10^{-14}$) between the model-estimated and experimentally derived rTAPL values in the macaque backbone network (density = 5%) (Fig. 2 *C* and *D*). Such a correlation was also observed under different connectivity densities (e.g., < 50%) of the macaque brain network across a range of α values [$\alpha \in (0.02, 0.18)$] (Fig. 2*E*). These results support the validity of this model for estimating the relative regional variation in the total axonal projection length of brain nodes in the primate structural connectome.

Using this weighted regional distance-dependent model, we estimated the regional total axonal projection length, rTAPL, of each brain node in the human backbone structural connectome (density = 3.5% within each hemisphere) (Fig. 3*A*). Here, we showed that the maximal correlation between estimated rTAPL and brain AG had the following values: left: $r = 0.42$, $P < 0.0001$ at $\alpha = 0.34$ and right: $r = 0.41$, $P < 0.0001$ at $\alpha = 0.34$ (Fig. 3*B*). Correlation significance was obtained using a spin test approach in which spatial autocorrelation was corrected (51). Significant correlations (all $P < 0.001$, spin tests) were also observed over a broad range of the control parameter $\alpha \in (0.18, 0.5)$ (Fig. 3*C*). Moreover, brain nodes with large estimated rTAPL values (top 30%) significantly overlapped with those having high AG (top 30%) (left: $Z = 4.32$, $P < 1.0 \times 10^{-5}$; right: $Z = 7.5$, $P < 1.0 \times 10^{-13}$; 10,000 permutation tests) (*SI Appendix*, section 3.4). These nodes are primarily distributed in the medial and lateral frontal and parietal regions. We also compared brain AG with traditionally defined wiring cost measures, including streamline number, streamline length, Euclidean distance, and combinations thereof (*SI Appendix*, Fig. S1). None of these traditionally defined wiring cost measures positively correlated with brain AG (all $P > 0.05$, Bonferroni-corrected) (*SI Appendix*, Fig. S1 and Table S1). These results suggest that brain AG as a metabolic measure significantly associates with the properly estimated regional total axonal projection lengths of the structural connectome.

Brain AG Significantly Mediates the Relationship between the Structural and Functional Connectomes. We further investigated the relationship between brain AG, estimated rTAPL, and functional integration in the human connectome. In brief, we first utilized HCP multiband rsfMRI data to generate a group-level functional connectome with 512 nodes for each hemisphere (*SI Appendix*, section 1.2). For each node, we then calculated its participation coefficient (28, 29) to quantify the extent of its functional integration in terms of its intermodule and intramodule connections (*SI Appendix*, section 4.1). Brain nodes with high participation coefficients (network connectors or gateways linking different functional modules, Fig. 3*D*) notably overlap with those having high AG and estimated rTAPL values (Fig. 3*A*). Scatterplots reveal that the participation coefficient of the functional connectome significantly correlates with brain AG (left: $r = 0.39$, $P < 0.0001$; right: $r = 0.33$, $P < 0.001$; spin tests) (Fig. 3*E*) and with the estimated rTAPL (left: $r = 0.25$, $P < 0.001$; right: $r = 0.24$, $P = 0.004$; spin tests).

Next, we performed a mediation analysis (52) to examine whether brain AG mediates the relationship between structural connectivity (measured by the estimated rTAPL) and functional integration (measured by the participation coefficient) (*SI Appendix*, section 4.2). For the left hemispheric network, we examined the total effects of 1) estimated rTAPL on functional integration (path c: $\beta = 0.01$; $P = 0.0001$); 2) estimated rTAPL on brain AG (path a: $\beta = 0.01$; $P < 0.0001$); and 3) brain AG on functional integration (path b: $\beta = 1.18$; $P < 0.0001$) (Fig. 3*F*). After controlling for brain AG, the direct effects of estimated rTAPL on functional integration became nonsignificant (path *c′*; $\beta = 0.003$; $P = 0.40$). Finally, bootstrap simulations ($n = 10{,}000$) also confirmed significant indirect effects of a × b for AG (95% confidence interval = [0.009, 0.016], $P < 0.0001$; Fig. 3*F*). Likewise, the mediation analysis revealed similar findings in the right hemispheric network (Fig. 3*F* and *SI Appendix*, Tables S2–S4). These results indicate that the regional total projection length of nodes in the structural connectome has an indirect effect on functional integration, which is significantly mediated through brain AG.

High-AG Regions Tend to Optimize Their Axonal Projection Lengths to Reduce Risk of Vulnerability. To determine whether the estimated total axonal projection lengths of high-AG regions are optimized

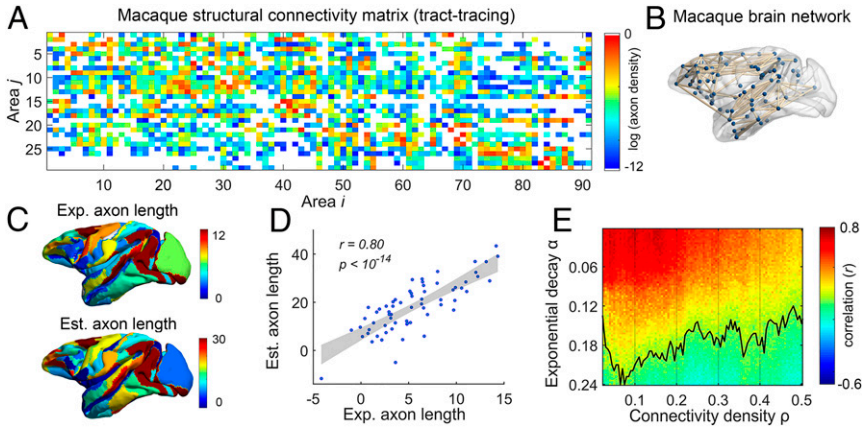

Fig. 2. Macroscopic macaque structural connectome and the estimation of total regional axonal projection length based on our proposed model. (*A*) The 91 × 29 structural connectivity matrix of the macaque brain network derived using tract-tracing technique (50). The connection weight between nodes *i* and *j*, i.e., the extrinsic fraction of labeled neurons (FLNe), was estimated as the ratio between the number of labeled neurons in node *i* and the total number of extrinsically labeled neurons in other nodes with an injection into node *j*. The connection weight indicates the normalized axonal projection number. For details, see ref. 50. (*B*) The macaque brain network was mapped on the cortical surface, with connections indicating axonal fiber density. (*C*, *Upper*) The experimental regional axonal projection lengths in the macaque brain network using tract-tracing technique. (*Bottom*) The estimated regional axonal projection lengths in the macaque brain network (connection density, 5%) based on our proposed weighted regional distance-dependent model. (*D*) Significant correlation was observed between the experimental and estimated regional axonal projection lengths in the macaque network. The measures were resampled into Gaussian distributions. This correlation was also significant without resampling ($r = 0.78$, $P < 1.0 \times 10^{-14}$). (*E*) Correlations between the experimental and estimated regional axonal projection lengths in the macaque brain networks under different connectivity density, ρ, and different exponential decay parameter, α, in the weighted distance-dependent model. The correlation values are significant with $P < 0.05$ when α is less than the boundary values shown by the black line.

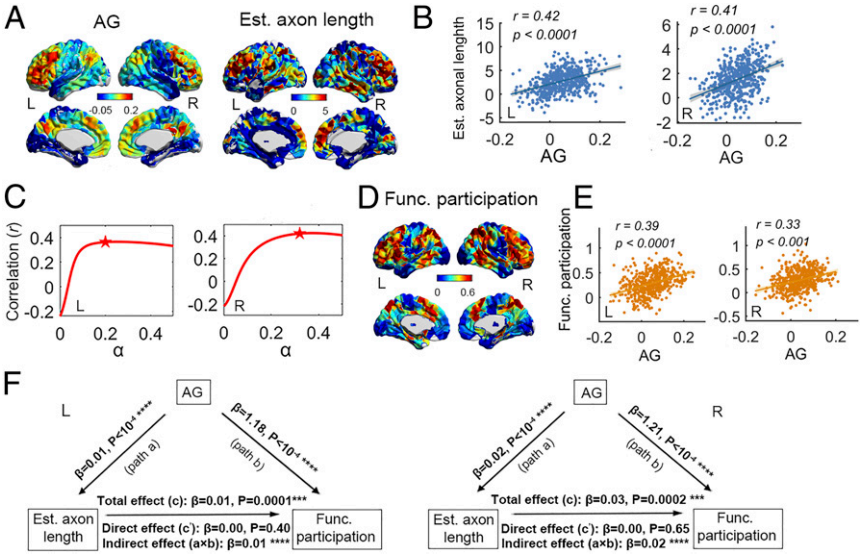

Fig. 3. Relationship between brain AG, estimated axonal projection length, and functional networks in the human connectome. (*A*) Maps of brain AG and estimated axonal projection length in the human brain. For each node, the total axonal projection length was estimated by applying our proposed weighted regional distance-dependent model to the structural connectome of the human brain derived from HARDI data. (*B*) Scatterplots revealed significant correlations between brain AG and estimated axon projection lengths. (*C*) The correlation curves between brain AG and estimated axonal projection lengths under different exponential decay parameter, α. The maximal correlation was marked with a red star for each hemispheric network, with scatterplots shown in *B*. (*D*) Participation coefficient values in the functional brain networks derived from rsfMRI data were mapped on the cortical surface. (*E*) Scatterplots revealed significant correlations between brain AG and participation coefficient values in the functional brain networks. (*F*) A mediation model of brain AG and the structural and functional connectomes for each hemispheric network. Brain AG serves as a significant mediator of the effect of estimated axonal projection lengths in the structural networks on the participation coefficient in the functional networks. **P* < 0.05, ***P* < 0.01, ****P* < 0.001, and *****P* < 0.0001. For *B* and *E*, we resampled the measures into Gaussian distributions. Spin tests, correcting for spatial autocorrelations, were conducted to confirm whether correlation significance was a result of chance. Pearson correlations and *P* values are shown in the figure. L, left hemisphere; R, right hemisphere.

to protect against the risk of vulnerability, we evaluated the extent of both wiring optimization and vulnerability risk in these regions by comparing the brain's structural connectome to optimized and randomized network models.

Using a simulated annealing algorithm, we first reconstructed a wiring-optimized network model in which the sum of estimated rTAPL values in the whole network was minimized while preserving the nodal degrees and nodal effective weights (which reflects the estimated normalized number of axonal projections of the node) in the actual brain network (*SI Appendix*, section 5.1). In this reconstructed network, each node tends to link with its short-range neighboring nodes to minimize their connection distance with the preservation of the heterogeneity of nodal degree. Thus, the network model is wiring economical and optimized, and simultaneously ensures an extent of network efficiency (53). For a given brain node *i*, we defined the extent of structural wiring optimization as the ratio of the estimated rTAPL value in the reconstructed optimized network to that in the actual brain network, $\text{Ratio}_i^{opt} = \text{rTAPL}_i^{opt}/\text{rTAPL}_i^{brain}$. We found that the highest levels of wiring optimization were primarily distributed in the medial and lateral prefrontal and parietal cortices (Fig. 4*A*), which corresponds very well to regions with elevated levels of AG (Fig. 1). These regions show Ratio_i^{opt} values closer to 1.0 (Fig. 4 *A* and *B*), implying that estimated total axonal lengths for these regions in the actual brain network display a high extent of optimization. Moreover, cross-node scatterplots revealed significant positive correlations between the level of wiring optimization, Ratio_i^{opt}, in the brain network and AG (left: $r = 0.38$, $P < 0.0001$; right: $r = 0.37$, $P < 0.0001$; spin tests) (Fig. 4*C*). Together, these results indicate that high-AG regions have almost fully optimized total axonal lengths, which is achieved through the predominance of short-range connections that link with neighboring nodes.

We also reconstructed two different randomized networks, without any constraints on estimated axonal projection lengths, by either randomly rewiring the links while maintaining fixed nodal degrees and nodal effective weights (link rewiring) or shuffling nodal placement while maintaining the fixed topological links (placement shuffling) in the structural brain network (*SI Appendix*, section 5.2). For each node *i*, we quantified the risk of increased rTAPL using two ratio values, being the ratio of the estimated rTAPL values in each of the random networks to those in the actual brain network: $\text{Ratio}_i^{link-rand} = \text{rTAPL}_i^{link-rand}/\text{rTAPL}_i^{brain}$ (link rewiring) and $\text{Ratio}_i^{place-rand} = \text{rTAPL}_i^{place-rand}/\text{rTAPL}_i^{brain}$ (placement shuffling). A high ratio value represents a hypothetically high risk of vulnerability in the absence of wiring optimization. We found that the highest risk of increased rTAPL occurred mainly in the medial and lateral prefrontal and parietal cortices (Fig. 4 *D* and *E*). Specifically, for high-AG regions (e.g., top 30%), the estimated rTAPL would increase more than fourfold if wiring or network node placement were randomized (Fig. 4 *F* and *G*). Cross-node scatterplots revealed that the hypothetical risk quantified by the two ratio measures positively correlated with brain AG ($\text{Ratio}_i^{link-rand}$: left: $r = 0.37$, $P < 0.0001$; right: $r = 0.36$, $P = 0.0001$; $\text{Ratio}_i^{place-rand}$: left: $r = 0.37$, $P < 0.0001$; right: $r = 0.34$, $P < 0.001$; spin tests) (Fig. 4 *H* and *I*). Together, in the absence of wiring optimization, high-AG regions would tend to have much longer axonal projection length than that observed in the actual human brain, which would demand even higher AG and potentially lead to higher risk of vulnerability. Thus, the topography of brain AG appears to manifest a benefit–risk mechanism in which both the demand of high metabolic requirements and the need to reduce risk of vulnerability are well balanced.

Discussion

In the present study, we reported the wiring mechanism behind brain AG topography. Specifically, we proposed a weighted

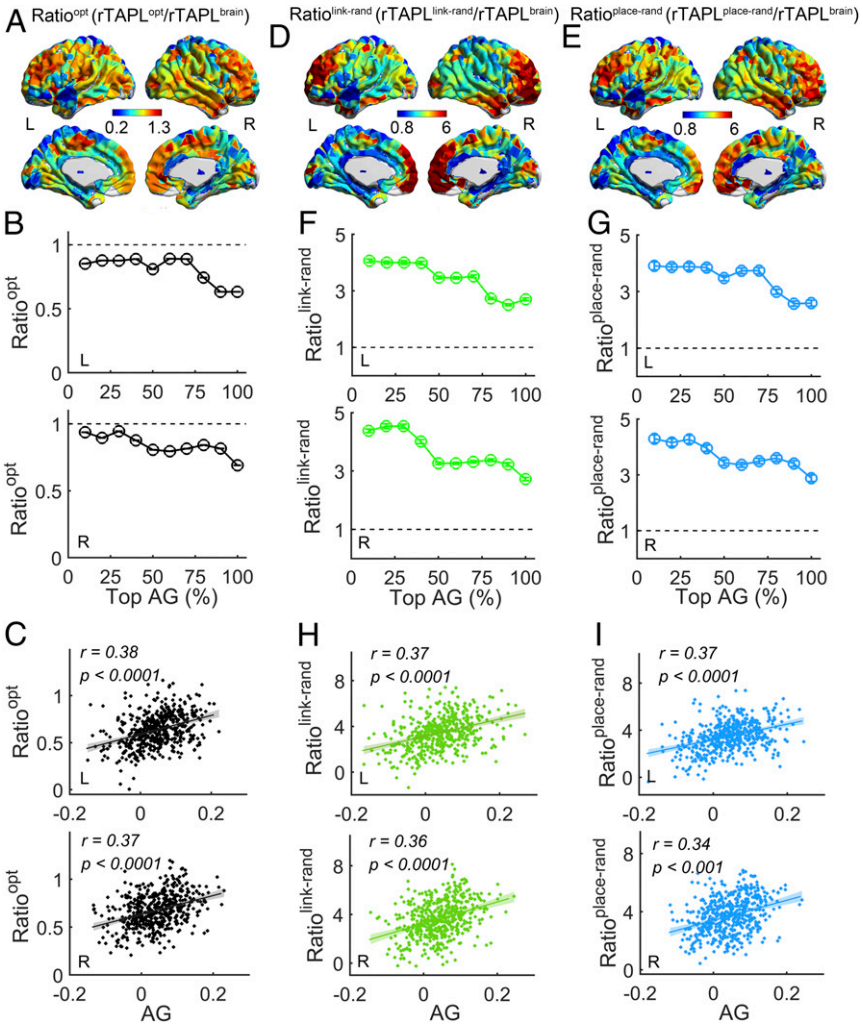

Fig. 4. The extent of wiring optimization and the risk of axonal length increase in the human structural connectome and their association with brain AG. (*A*) Spatial maps of the extent of wiring optimization, Ratio^{opt}, based on comparisons of the reconstructed optimized network and the human brain structural network. (*B*) Mean Ratio^{opt} values change with the proportion of top AG values. Notably, mean Ratio^{opt} values are closer to 1 in high-AG regions (e.g., top 30%), suggesting optimized axonal projection lengths in these regions. (*C*) Scatterplots revealed significant correlations between brain AG and Ratio^{opt}. (*D* and *E*) Spatial maps of the risk of increased regional total axonal projection length, Ratio$^{link-rand}$ and Ratio$^{place-rand}$, based on comparisons of the reconstructed random networks and the human brain structural network. (*F* and *G*) Mean Ratio$^{link-rand}$ and Ratio$^{place-rand}$ values change with the proportion of top AG values. Notably, the estimated total axonal projection length in high-AG regions (e.g., top 30%) would increase more than fourfold in randomized networks (i.e., without wiring optimization). (*H* and *I*) Scatterplots revealed significant correlations between brain AG and Ratio$^{link-rand}$ and Ratio$^{place-rand}$. For *C*, *H*, and *I*, we resampled the measures into Gaussian distributions. Pearson correlations and *P* values, following spin tests, are shown in the figure. L, left hemisphere; R, right hemisphere.

regional distance-dependent model to approximately capture the total axonal projection length of a given brain node. Our results delineate a tight association between brain AG and the regional wiring cost of the structural connectome. High-AG regions, which are primarily distributed in the medial and lateral prefrontal and parietal cortices, exhibit a high extent of optimization in their total axonal length, allowing the risk of vulnerability to be reduced. These results reveal a benefit–risk balancing mechanism in the human brain and provide insights into understanding the relationship between brain metabolism and connectome.

The normal functioning of the brain is supported not only by structural wiring (53, 54) but also by metabolism such as AG (6, 8). However, the relationship between wiring cost and metabolism in the brain remains unclear. Here, we showed that AG levels are associated with the estimated total axonal projection length of brain nodes in the structural connectome. At a microscopic level, AG provides metabolic functions including biosynthesis and ATP generation, which are critical for axons with myelin (9, 19–21). Specifically, glycolytic product is the precursor for biosynthesis in myelination (15, 16) and axonal elongation (17). High-AG regions are enriched for genes involved in the regulation of axon guidance and synaptic plasticity (11, 18). Moreover, oligodendroglia glycolytic support is crucial for long-term axonal integrity (9, 19, 20). Toxic molecules such as amyloid-β affect the oligodendroglia as a transporter of glycolysis, degrading their ability to maintain axon viability (9, 21, 26). In terms of energy metabolism, AG is an important pathway for the rapid supply of ATP. Several studies on astrocyte–neuron lactate shuttles suggest that AG supplies the energy demands of Na^+/K^+ ATPase membrane pumps (26, 55). Given that the number of Na^+/K^+ pumps is proportional to axon area (56) and that axon diameter shows relatively little variation (57), the level of ATP production-related brain AG is proportional to axonal length. Together, the above microscale evidence provides strong support for our finding of the tight relationship between AG levels

and regional total axonal projection length. Notably, regions with high AG and long axonal lengths are primarily distributed in the transmodal areas. However, a recent study has suggested that these areas do not contain heavy myelin content (58). This could be due to the estimation of myelin content being performed in gray matter, using the ratio of T1/T2-weighted MR images. Future studies are needed to measure the true length of regional axonal projections using novel experimental approaches, and to further elucidate the relationship between axonal length and brain AG.

Several recent studies have demonstrated the association between brain AG and the network topology of the human connectome. Specifically, brain AG values are higher in densely connected hubs and rich-club structures than in other regions (1, 27). In the present study, we highlighted the tight relationship between brain AG as a running cost and estimated total axonal projection length as a wiring cost in the human connectome. Moreover, one advantage that our findings offer when compared to the network topology approach is that it provides a unique opportunity to understand how a balancing of the benefits and risks of AG is achieved by the optimal organization of structural wiring diagrams in the human brain. Importantly, the model that we have proposed is a weighted regional distance-dependent model, which estimates the total axonal length of each brain node in the structural connectome. This model was developed primarily considering the fact that connection weights (e.g., streamline number) derived from noninvasive diffusion MRI data cannot properly capture the number of axon projections (42, 46, 47). Previous studies of macaque connectomes demonstrated that axon projection number follows an exponential decay with connection distance (Euclidean distance) statistically, suggesting delicately tuned connectional weights between regions (48, 50). However, there is a large variation in experimental weights for long-distance connections, which may cause errors when the regional total axonal projection length is estimated by summing all products of connection weight multiplied by Euclidean distance. If predicted connection weights based on an exponential rule (48) are utilized to estimate regional total axonal projection length of brain nodes, the resultant values do not correlate with the experimental measurements (*SI Appendix*, Fig. S2). Thus, in this work, we proposed a computational model based on two critical factors of the structural connectome, the binary interregional connections and their Euclidean distances. For a given nodal region, its weight in the model is acquired by estimating not the internode connectional weights but the regional effective weight (i.e., normalized axonal projection number) through exponentially fitting the average Euclidean distance of the connections linking the node. In this case, the model captures the statistical feature of exponential decay of weight with connection distance and allows for large fluctuations of individual connections within the distance bins. Notably, this model provides appropriate estimations of the total axonal length of brain nodes in a macaque network derived from tract-tracing data (*SI Appendix*, Fig. S3). Using this model, we reported that brain AG had significant positive correlations with the estimated regional total axonal projection length, rather than with traditionally defined wiring costs (e.g., the streamline number) derived from diffusion MRI data. Moreover, the range of the control parameters in this model is similar between the human and macaque networks, suggesting the feasibility of using the proposed computational model in estimating the regional total axonal projection length of the primate connectome. For validation, we also calculated regional total axonal projection length under the same model using the geodesic distance in the human connectome derived from diffusion MRI tractography in place of Euclidean distance (*SI Appendix*, section 7). We found that the newly estimated regional total axonal projection lengths were highly correlated with those estimated based on Euclidean distance (left: $r = 0.94$, $P < 1.0 \times 10^{-15}$; right: $r = 0.97$, $P < 1.0 \times 10^{-15}$) and also highly correlated with brain AG (left: $r = 0.47$, $P < 0.0001$; right: $r = 0.42$, $P < 0.0001$; *SI Appendix*, Fig. S8). Due to the lack of geodesic distance data in the randomized and optimized networks used as comparison sets against real brain data, we have used Euclidean distance in our model to maintain the consistency of our work.

One interesting observation in the present study is that brain AG mediates the relationship between structural wiring and functional integration. Numerous works suggest that the functional network of the brain is anatomically constrained by the underlying structural network (2, 59). However, the metabolic role of brain AG in structural–functional coupling remains unclear. High-AG regions are mainly distributed in the default-mode network that is associated with self-referential processing and episodic memory processing (6), and the frontoparietal network that is associated with task control processes (30). Some of these regions play a central role in global communication as brain hubs (29, 30) and have a high glucose metabolic rate (60, 61). These high-AG regions tend to project high weighted connections (*SI Appendix*, Fig. S4) and have a large number of interregional axon projections overall (*SI Appendix*, Fig. S7) to support the large computational load of integrating multiple functional systems. Moreover, AG can be linked with neuronal firing activity (62). These studies provide support for our finding that brain AG plays a role in mediating the structural–functional relationship. Several studies have reported that brain AG declines with normal aging (34) and in AD (63). This reduction of AG could mean that AG levels become insufficient to support the axons, thus leading to reduced fiber integrity and thereby impacting structural–functional coupling in patients (64). We believe that elucidating the relationship between metabolism and the structural and functional connectomes in the brain will boost more studies to deepen our understanding of network dysfunctions in brain disorders in which metabolism levels are often insufficient.

It is important to note that high-AG regions exhibit optimized structural wiring to reduce the risk of vulnerability. As a networked biological system, the brain is likely to have evolved a mechanism that balances the trade-off between benefits and risks. On the one hand, functional integration of high-order regions (e.g., default-mode and frontoparietal systems) requires high AG to support the metabolic demands of a large number of axon projections. On the other hand, elevated levels of AG are closely associated with higher risk of amyloid-β deposition (13, 14). Previous works suggest that AG is critical for task-induced activity (10) and synaptic plasticity (11). However, mouse brain studies also suggest an association between neuronal activity, lactate levels, and amyloid-β content (32, 33). In the aging human brain, the topography of brain AG flattens with normal aging (34) and in AD (63), with the greatest decline in regions with high AG during young adulthood. Since AG protects the brain from reactive oxygen species and prevents oxidative stress (12, 35, 36), it would be more challenging for these originally higher AG regions to maintain protection against reactive oxygen species in aging. At the same time, oxidative stress is closely related to the accumulation of amyloid-β (35), which affects the glycolytic oligodendrocytes (9, 21, 26). This vicious cycle exacerbates the pathogenic process, potentially leading to AD (36, 65). Furthermore, high-AG regions correspond to those that are commonly attacked by various brain disorders (66–68). Using reconstructed network models, we demonstrated that connectivity wiring in these high-AG regions are designed to balance the benefit of functional integration with the mitigation of exposure to higher risk. Specifically, high-AG regions tend to project connections to their nearest neighboring regions, so that their total axonal projection lengths are nearly minimized. In contrast, randomly rewiring the connections or randomly situating nodal locations would cause a greater increase in the total

axonal projection length of high-AG regions than in others. Interestingly, we also found that the extent to which regional total axonal projection length is optimized is significantly correlated with AG (Fig. 4), and not with oxygen ($P = 0.84$). This corresponds with previous works showing that high AG, rather than high oxygen, is closely associated with the critical vulnerability factor to amyloid-β deposition (12, 36). In summary, high-AG regions have rich axon projections to meet their functional requirements, and simultaneously reduce the risk of vulnerability by projecting connections to neighboring regions, suggesting a trade-off mechanism that balances benefit and risk in the human brain.

Several issues need to be further addressed. First, there is currently a lack of techniques for the collection of data on true interregional axonal projections in the human brain. Thus, we proposed a computational model to estimate the total axonal projection length of each brain node. This model has been validated in a macaque connectome derived from tract-tracing data (Fig. 2). In this study, we also validated the model against mouse connectome data derived using two-photon tomography techniques (69). We observed a significant correlation ($r = 0.76$, $P < 1.0 \times 10^{-15}$) between the estimated and experimental regional total axonal projection lengths in the mouse connectome (connectivity density, 30%) (for details, see *SI Appendix*, section 8). These results suggest that the proposed model may be appropriate for estimating regional total axonal projection length in the connectome of different species. However, it should be noted that this model is based on Euclidean distance, which is only valid for intrahemispheric networks. Interhemispheric connections cannot be included in this model due to the large deviation between the axonal projection length and Euclidean distance between regions across the two hemispheres. In the future, it will be important to precisely measure the length of axon projections in the human brain by developing advanced imaging techniques and computational modeling. Second, the structural connectome of the human brain derived from diffusion MRI data and deterministic tractography approaches does not include direction information. As mentioned previously, brain AG supports axonal growth and synapse activity (9, 19, 20, 26, 70). If AG predominantly supports axonal growth and integrity, AG levels would be expected to be high at regions that emit projections. If AG predominantly supports synapse activity, it would be expected to be high at regions that receive a large number of input projections, especially at regions with many multisynaptic connections. In the future, the directional structural brain networks would be helpful for investigations exploring which of the two AG plays a greater part in. Third, our results suggest that optimal structural wiring in high-AG regions effectively reduces the potential risk of vulnerability. To verify this point, further studies need to be conducted to explore whether less optimal wiring in the high-AG regions induces higher risk of vulnerability, for example, by testing whether the estimated total axonal length of these regions are higher in individuals who later develop brain disorders (e.g., AD) than in those who remain healthy. Specifically, these issues can be addressed by combining PET and connectome data as well as computational modeling.

Materials and Methods

Participants and Data Acquisition. Two neuroimaging datasets were included in the current study. Dataset 1 comprised PET data from 33 healthy, right-handed participants (19 females and 14 males; mean age, 25.4 ± 2.6 y) who were recruited from the Washington University community (6). The scans were performed on a Siemens model 961 ECAT EXACT 47 PET scanner (Siemens/CTI) to measure the cerebral metabolic rate of glucose (CMRGlu), oxygen (CMR O_2) and AG. Dataset 2 comprised multimodal MRI data from 38 healthy right-handed participants, including multishell HARDI and rsfMRI data, which was obtained from the WU-Minn HCP database (https://db.humanconnectome.org, "unrelated 40 subjects") (39). All participants underwent structural, functional, and diffusion MRI scanning in a customized Siemens 3T Connectome Skyra scanner using a 32-channel head coil at Washington University.

Data Analysis. Both PET and MRI data were preprocessed using standard pipelines. After this, we measured brain AG levels and reconstructed the structural and functional connectomes of the human brain based on a random parcellation with 1,024 nodes (40). Network analysis and AG–connectome association analysis was performed as follows. 1) To estimate the total axonal projection length of each brain node, we developed a weighted distance-dependent model. This model was validated in a macaque connectome derived from tract-tracing data. 2) We applied the above model to the structural connectome of the human brain derived from HCP HARDI data to estimate the regional total axonal projection length for each node, followed by an association analysis with brain AG. 3) We evaluated the role of brain nodes in functional integration by calculating their participation coefficients among different modules in the functional connectome obtained from HCP rsfMRI data. A mediation analysis was further conducted to elucidate the relationship between brain AG, the structural connectome, and the functional connectome. 4) We used a simulated annealing algorithm to generate a wiring-optimized network. We also generated two randomized networks by rewiring the links based on the structural connectome of the human brain. For each brain node, we further evaluated the extent of wiring optimization and the extent of axonal length increase using two ratios, being respectively the ratio of the estimated regional total axonal projection length in the optimized network or the random networks to that in the actual brain network.

Further details regarding the participants, data acquisition, data preprocessing, and data analyses are described in *SI Appendix*.

Data Availability. Some study data applied in this work have been deposited on GitHub, https://github.com/sofia1423/YuhanChen.github.io.git, which includes the human structural and functional connectomes, the macaque structural connectome, and the mouse structural connectome. All data related to this paper are included in the article and *SI Appendix*.

ACKNOWLEDGMENTS. We thank Prof. Marcus Raichle for generously sharing the PET data and for his invaluable suggestions, and Drs. Russ Hornbeck and Lars Couture for their help in the PET data analysis, Dr. Xindi Wang for his help in statistical analysis, Dr. Xiaochen Sun for her help in mediation analysis, and Drs. Mingrui Xia, Tengda Zhao, and Dingna Duan for helpful discussion. This work was supported by the Natural Science Foundation of China (Grants 81620108016, 81601560, 82021004, 31830034, 11328501, 11275027, 11975194, and 81971690), National Key Research and Development Project (Grant 2018YFA0701402), the Changjiang Scholar Professorship Award (Grant T2015027), the Hong Kong Research Grant Council (Grants HKBU12302914 and HKBU12200217), Hong Kong Baptist University (HKBU) Faculty Research Grant (FRG2/17-18/011), and the HKBU Research Committee Interdisciplinary Research Clusters Matching Scheme (IRCMs/18-19/SCI01).

1. E. Bullmore, O. Sporns, The economy of brain network organization. *Nat. Rev. Neurosci.* **13**, 336–349 (2012).
2. H. J. Park, K. Friston, Structural and functional brain networks: From connections to cognition. *Science* **342**, 1238411 (2013).
3. B. J. Shannon *et al.*, Brain aerobic glycolysis and motor adaptation learning. *Proc. Natl. Acad. Sci. U.S.A.* **113**, E3782–E3791 (2016).
4. X. Liao, A. V. Vasilakos, Y. He, Small-world human brain networks: Perspectives and challenges. *Neurosci. Biobehav. Rev.* **77**, 286–300 (2017).
5. P. J. Magistretti, I. Allaman, Lactate in the brain: From metabolic end-product to signalling molecule. *Nat. Rev. Neurosci.* **19**, 235–249 (2018).
6. S. N. Vaishnavi *et al.*, Regional aerobic glycolysis in the human brain. *Proc. Natl. Acad. Sci. U.S.A.* **107**, 17757–17762 (2010).
7. K. De Bock *et al.*, Role of PFKFB3-driven glycolysis in vessel sprouting. *Cell* **154**, 651–663 (2013).
8. A. L. Bauernfeind *et al.*, Aerobic glycolysis in the primate brain: Reconsidering the implications for growth and maintenance. *Brain Struct. Funct.* **219**, 1149–1167 (2014).
9. U. Fünfschilling *et al.*, Glycolytic oligodendrocytes maintain myelin and long-term axonal integrity. *Nature* **485**, 517–521 (2012).
10. A. G. Vlassenko, M. E. Raichle, Brain aerobic glycolysis functions and Alzheimer's disease. *Clin. Transl. Imaging* **3**, 27–37 (2015).
11. M. S. Goyal, M. Hawrylycz, J. A. Miller, A. Z. Snyder, M. E. Raichle, Aerobic glycolysis in the human brain is associated with development and neotenous gene expression. *Cell Metab.* **19**, 49–57 (2014).
12. K. A. Brand, U. Hermfisse, Aerobic glycolysis by proliferating cells: A protective strategy against reactive oxygen species. *FASEB J.* **11**, 388–395 (1997).
13. M. S. Goyal *et al.*, Spatiotemporal relationship between subthreshold amyloid accumulation and aerobic glycolysis in the human brain. *Neurobiol. Aging* **96**, 165–175 (2020).

14. A. G. Vlassenko *et al*., Spatial correlation between brain aerobic glycolysis and amyloid-β (Aβ) deposition. *Proc. Natl. Acad. Sci. U.S.A.* **107**, 17763–17767 (2010).
15. A. M. Brown, R. Wender, B. R. Ransom, Metabolic substrates other than glucose support axon function in central white matter. *J. Neurosci. Res.* **66**, 839–843 (2001).
16. S. B. Tekkök, A. M. Brown, R. Westenbroek, L. Pellerin, B. R. Ransom, Transfer of glycogen-derived lactate from astrocytes to axons via specific monocarboxylate transporters supports mouse optic nerve activity. *J. Neurosci. Res.* **81**, 644–652 (2005).
17. D. L. Nelson, A. L. Lehninger, M. M. Cox, *Lehninger Principles of Biochemistry* (Macmillan, 2008).
18. J. L. Goldberg, How does an axon grow? *Genes Dev.* **17**, 941–958 (2003).
19. Y. Lee *et al*., Oligodendroglia metabolically support axons and contribute to neurodegeneration. *Nature* **487**, 443–448 (2012).
20. A. S. Saab, K. A. Nave, Myelin dynamics: Protecting and shaping neuronal functions. *Curr. Opin. Neurobiol.* **47**, 104–112 (2017).
21. A. S. Saab, I. D. Tzvetanova, K. A. Nave, The role of myelin and oligodendrocytes in axonal energy metabolism. *Curr. Opin. Neurobiol.* **23**, 1065–1072 (2013).
22. L. M. Supplie *et al*., Respiration-deficient astrocytes survive as glycolytic cells in vivo. *J. Neurosci.* **37**, 4231–4242 (2017).
23. A. Volkenhoff *et al*., Glial glycolysis is essential for neuronal survival in *Drosophila*. *Cell Metab.* **22**, 437–447 (2015).
24. R. Medori, L. Autilio-Gambetti, S. Monaco, P. Gambetti, Experimental diabetic neuropathy: Impairment of slow transport with changes in axon cross-sectional area. *Proc. Natl. Acad. Sci. U.S.A.* **82**, 7716–7720 (1985).
25. J. W. Griffin, D. F. Watson, Axonal transport in neurological disease. *Ann. Neurol.* **23**, 3–13 (1988).
26. K. A. Nave, Myelination and the trophic support of long axons. *Nat. Rev. Neurosci.* **11**, 275–283 (2010).
27. G. Collin, O. Sporns, R. C. Mandl, M. P. van den Heuvel, Structural and functional aspects relating to cost and benefit of rich club organization in the human cerebral cortex. *Cereb. Cortex* **24**, 2258–2267 (2014).
28. Y. He *et al*., Uncovering intrinsic modular organization of spontaneous brain activity in humans. *PLoS One* **4**, e5226 (2009).
29. M. P. van den Heuvel, O. Sporns, Network hubs in the human brain. *Trends Cogn. Sci.* **17**, 683–696 (2013).
30. M. A. Bertolero, B. T. Yeo, M. D'Esposito, The modular and integrative functional architecture of the human brain. *Proc. Natl. Acad. Sci. U.S.A.* **112**, E6798–E6807 (2015).
31. M. P. van den Heuvel, O. Sporns, An anatomical substrate for integration among functional networks in human cortex. *J. Neurosci.* **33**, 14489–14500 (2013).
32. S. L. Macauley *et al*., Hyperglycemia modulates extracellular amyloid-β concentrations and neuronal activity in vivo. *J. Clin. Invest.* **125**, 2463–2467 (2015).
33. A. W. Bero *et al*., Neuronal activity regulates the regional vulnerability to amyloid-β deposition. *Nat. Neurosci.* **14**, 750–756 (2011).
34. M.S. Goyal *et al*., Loss of brain aerobic glycolysis in normal human aging. *Cell Metab.* **26**, 353–360.e3 (2017).
35. S. Mondragón-Rodríguez *et al*., Phosphorylation of tau protein as the link between oxidative stress, mitochondrial dysfunction, and connectivity failure: Implications for Alzheimer's disease. *Oxid. Med. Cell. Longev.* **2013**, 940603 (2013).
36. E. Tönnies, E. Trushina, Oxidative stress, synaptic dysfunction, and Alzheimer's disease. *J. Alzheimers Dis.* **57**, 1105–1121 (2017).
37. K. P. Kepp, A quantitative model of human neurodegenerative diseases involving protein aggregation. *Neurobiol. Aging* **80**, 46–55 (2019).
38. A. G. Vlassenko *et al*., Aerobic glycolysis and tau deposition in preclinical Alzheimer's disease. *Neurobiol. Aging* **67**, 95–98 (2018).
39. D. C. Van Essen *et al*.; WU-Minn HCP Consortium, The WU-Minn human connectome project: An overview. *Neuroimage* **80**, 62–79 (2013).
40. A. Zalesky *et al*., Whole-brain anatomical networks: Does the choice of nodes matter? *Neuroimage* **50**, 970–983 (2010).
41. B. T. Yeo *et al*., The organization of the human cerebral cortex estimated by intrinsic functional connectivity. *J. Neurophysiol.* **106**, 1125–1165 (2011).
42. Roberts *et al*., The contribution of geometry to the human connectome. *Neuroimage* **124**, 379–393 (2016).
43. X. Wang, Q. Lin, M. Xia, Y. He, Differentially categorized structural brain hubs are involved in different microstructural, functional, and cognitive characteristics and contribute to individual identification. *Hum. Brain Mapp.* **39**, 1647–1663 (2018).
44. E. T. Bullmore, D. S. Bassett, Brain graphs: Graphical models of the human brain connectome. *Annu. Rev. Clin. Psychol.* **7**, 113–140 (2011).
45. M. P. van den Heuvel, R. S. Kahn, J. Goñi, O. Sporns, High-cost, high-capacity backbone for global brain communication. *Proc. Natl. Acad. Sci. U.S.A.* **109**, 11372–11377 (2012).
46. D. K. Jones, Challenges and limitations of quantifying brain connectivity in vivo with diffusion MRI. *Imaging Med.* **2**, 341–355 (2010).
47. D. K. Jones, T. R. Knösche, R. Turner, White matter integrity, fiber count, and other fallacies: The do's and don'ts of diffusion MRI. *Neuroimage* **73**, 239–254 (2013).
48. M. Ercsey-Ravasz *et al*., A predictive network model of cerebral cortical connectivity based on a distance rule. *Neuron* **80**, 184–197 (2013).
49. H. F. Song, H. Kennedy, X. J. Wang, Spatial embedding of structural similarity in the cerebral cortex. *Proc. Natl. Acad. Sci. U.S.A.* **111**, 16580–16585 (2014).
50. N. T. Markov *et al*., A weighted and directed interareal connectivity matrix for macaque cerebral cortex. *Cereb. Cortex* **24**, 17–36 (2014).
51. A. F. Alexander-Bloch *et al*., On testing for spatial correspondence between maps of human brain structure and function. *Neuroimage* **178**, 540–551 (2018).
52. A. F. Hayes, *Introduction to Mediation, Moderation, and Conditional Process Analysis: A Regression-Based Approach* (Guilford Publications, 2017).
53. Y. Chen, S. Wang, C. C. Hilgetag, C. Zhou, Features of spatial and functional segregation and integration of the primate connectome revealed by trade-off between wiring cost and efficiency. *PLoS Comput. Biol.* **13**, e1005776 (2017).
54. A. Avena-Koenigsberger, B. Misic, O. Sporns, Communication dynamics in complex brain networks. *Nat. Rev. Neurosci.* **19**, 17–33 (2017).
55. L. F. Barros, Metabolic signaling by lactate in the brain. *Trends Neurosci.* **36**, 396–404 (2013).
56. S. B. Laughlin, R. R. de Ruyter van Steveninck, J. C. Anderson, The metabolic cost of neural information. *Nat. Neurosci.* **1**, 36–41 (1998).
57. R. Olivares, J. Montiel, F. Aboitiz, Species differences and similarities in the fine structure of the mammalian corpus callosum. *Brain Behav. Evol.* **57**, 98–105 (2001).
58. M. F. Glasser, D. C. Van Essen, Mapping human cortical areas in vivo based on myelin content as revealed by T1- and T2-weighted MRI. *J. Neurosci.* **31**, 11597–11616 (2011).
59. B. Mišić *et al*., Network-level structure-function relationships in human neocortex. *Cereb. Cortex* **26**, 3285–3296 (2016).
60. X. Liang, Q. Zou, Y. He, Y. Yang, Coupling of functional connectivity and regional cerebral blood flow reveals a physiological basis for network hubs of the human brain. *Proc. Natl. Acad. Sci. U.S.A.* **110**, 1929–1934 (2013).
61. D. Tomasi, G. J. Wang, N. D. Volkow, Energetic cost of brain functional connectivity. *Proc. Natl. Acad. Sci. U.S.A.* **110**, 13642–13647 (2013).
62. A. S. Saab *et al*., Oligodendroglial NMDA receptors regulate glucose import and axonal energy metabolism. *Neuron* **91**, 119–132 (2016).
63. M. Á. Araque Caballero *et al*., White matter diffusion alterations precede symptom onset in autosomal dominant Alzheimer's disease. *Brain* **141**, 3065–3080 (2018).
64. Z. Dai *et al*., Disrupted structural and functional brain networks in Alzheimer's disease. *Neurobiol. Aging* **75**, 71–82 (2019).
65. G. B. Stokin *et al*., Axonopathy and transport deficits early in the pathogenesis of Alzheimer's disease. *Science* **307**, 1282–1288 (2005).
66. N. A. Crossley *et al*., The hubs of the human connectome are generally implicated in the anatomy of brain disorders. *Brain* **137**, 2382–2395 (2014).
67. H. Oh, C. Madison, S. Baker, G. Rabinovici, W. Jagust, Dynamic relationships between age, amyloid-β deposition, and glucose metabolism link to the regional vulnerability to Alzheimer's disease. *Brain* **139**, 2275–2289 (2016).
68. Z. Sha, T. D. Wager, A. Mechelli, Y. He, Common dysfunction of large-scale neurocognitive networks across psychiatric disorders. *Biol. Psychiatry* **85**, 379–388 (2019).
69. S. W. Oh *et al*., A mesoscale connectome of the mouse brain. *Nature* **508**, 207–214 (2014).
70. E. Bufill, J. Agustí, R. Blesa, Human neoteny revisited: The case of synaptic plasticity. *Am. J. Hum. Biol.* **23**, 729–739 (2011).